Nondestructive diagnostics for relativistic picosecond bunched electron beams

J. C. Swartz
Department of Physics, Duke University, Durham, North Carolina 27708-0305

B. D. Guenther
Physics Division, U.S. Army Research Office, Research Triangle Park, North Carolina 27709

F. C. De Lucia and Wei Guo
Department of Physics, The Ohio State University, Columbus, Ohio 43210

C. R. Jones, H. Kosai, and J. M. Dutta
Department of Physics, North Carolina Central University, Durham, North Carolina 27707
(Received 20 April 1995)

The duration and form of relativistic picosecond electron bunches in the Duke University Mark III free-electron laser have been nondestructively measured by monitoring the submillimeter radiation produced by the bunches as they pass by or through a rectangular waveguide. Unlike other methods, our technique produces negligible electron bunch perturbation and allows real-time beam diagnostics to be performed simultaneously with free-electron laser (FEL) operation. We have measured 2.1-ps full width at half maximum duration electron bunches, studied the effect of electron gun and FEL modifications on bunch duration, and observed electron bunch variations during bunch trains.

PACS number(s): 41.85.Ew, 41.85.Qg, 41.75.Ht, 41.60.Cr

INTRODUCTION

Relativistic beams of bunched electrons are found in microwave sources such as transition radiation and Cherenkov devices, optical sources such as free-electron lasers, and particle sources such as linear accelerators. In many of these applications the pulse performance of the electron source is critical to the overall system operation; nonetheless, very few pulsed electron beam diagnostics are available. Traditional diagnostics either lack subpicosecond temporal resolution or interact destructively with the electron beam. Often the final system output [e.g., free-electron laser (FEL) output power] is the sole parameter by which the electron beam is adjusted. If better, more direct electron beam analysis tools were available, the bunched electron beam system operation could be greatly improved.

This paper will demonstrate a nondestructive technique of analyzing the picosecond temporal characteristics of a bunched relativistic electron beam. Results will show the measurement of a picosecond electron bunch and the real-time measurement of electron bunch parameters during an electron beam system adjustment.

I. BACKGROUND

Several different methods have been used to characterize relativistic bunched electron beams. Various rf pickups [1–9] (loop antenna, stripline coupling structure, or resonant cavity pickup) can detect the electromagnetic (e.m.) transient generated by an electron bunch as it passes the probe location without perturbing the beam. These probes are typically used as beam position monitors (BPMs) and their temporal resolution are limited by geometry and electronics to a few nanoseconds. Therefore, the time response of a BPM is restricted to monitoring the temporal evolution of *trains* of electron bunches and not the individual electron bunch.

Synchrotron radiation monitors are based on the fact that a relativistic electron beam radiates a narrow cone of radiation as the beam is accelerated (e.g., by turning magnets) [10–12]. By using appropriate optical detector arrays, researchers have used synchrotron radiation from relativistic electron bunches [1,3,13,14] as a means of determining the electron beam position. However, the response time of typical detector arrays is greater than 1 ns, preventing temporal measurement of the picosecond bunch.

Various groups have measured the transition [15–17] and Cherenkov radiation [18] emitted by relativistic electron bunches to determine bunch duration. Because these techniques destroy the electron bunch during measurement, they are not applicable to real-time diagnostics.

Although widely used, traditional electron beam monitoring techniques have poor temporal resolution and may destroy the electron beam they seek to measure. However, a simple extension of the BPM concept allows the use of a Fourier transform spectroscopic techniques to measure the electron beam transient and determine the pulse shape and width. The theory and experimental results of such a measurement are developed in the following sections.

II. THEORY

This section develops a model of the signals produced by a bunched relativistic electron beam and subsequently measured by the Fourier transform spectrometer. Based on this model, the signal measured by the spectrometer is related to the electron bunch parameters. Two experimental geometries were used to nondestructively sample the wide bandwidth field produced by the bunched electron beam: in one geometry, the electron beam travels axially through the center of a conductive pipe, exciting a small waveguide antenna (pickup) in the pipe wall (Fig. 1); in the other geometry, the electron beam crosses a rectangular waveguide (pickup), exciting waveguide rf modes (Fig. 2). Early experiments used a circular waveguide located at a ceramic break in the beam line as an rf pickup; however, the rectangular waveguide pickup yielded a coupling structure more easily analyzed and implemented. In all cases, the rf from the pickup waveguide is transported, by overmoded waveguide and free space optics, to a Fourier transform spectrometer for analysis. This section will present theoretical models used to analyze the system operation.

A. Field sampling: The electron beam crossing the rectangular waveguide

For the case of the electron bunch crossing the rectangular waveguide, the electron beam couples energy into the waveguide mode when the waveguide mode oscillation decelerates the electrons. Assuming a uniform field E_y across the waveguide, the total energy transferred $\langle S(\omega)\rangle$ into a mode of frequency ω and phase ϕ is

$$\langle S(\omega)\rangle \propto \frac{1}{\tau_t}\int_{t=-\tau_t/2}^{\tau_t/2}\cos(\omega t+\phi)dt$$
$$=\frac{\sin(\omega\tau_t/2+\phi)+\sin(\omega\tau_t/2-\phi)}{\omega\tau_t}$$
$$=\frac{\sin(\omega\tau_t/2)\cos(\phi)}{\omega\tau_t/2}, \quad (1)$$

where the transit time τ_t is the time required for the electron to cross the waveguide. If the transit time is too long, energy coupled from the electron beam during an early part of the beam transit is returned during a later part of the transit.

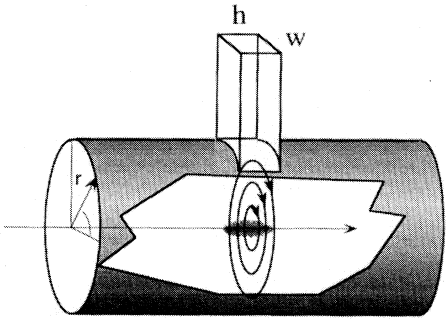

FIG. 1. Waveguide geometry for the coupling rf from a cylindrical electron beam pipe into a rectangular pickup with height h and width w.

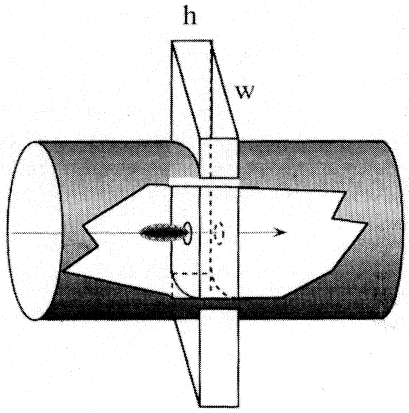

FIG. 2. Waveguide geometry for the coupling rf from an electron bunch traversing a rectangular waveguide with height h and width w.

The result is that the pickup waveguide will couple a field whose time evolution (and frequency content) is initially that of the bunched electron beam. However, the waveguide cutoff imposes a low-frequency limit on the transmitted signal, whereas beam transit time effects impose a high-frequency limit.

In addition, waveguide attenuation and dispersion distort the rf signal as it propagates from the electron beam system to the analysis instruments. When examining the actual measured data all these effects should be considered and may require compensation in a final pulse analysis.

B. Non-negligible beamwidth coupling effect

The traditional waveguide coupling analysis assumes that the transverse dimension of the electron beam is infinitesimally narrow compared to a wavelength [Fig. 3(a)]. However, for small waveguide dimensions and for the electron beam dimensions used in this experiment,

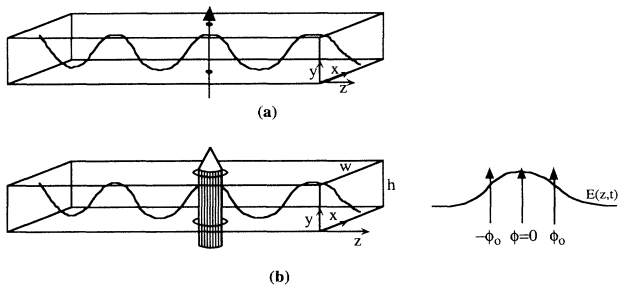

FIG. 3. Geometry for the coupling electron beam energy into a waveguide mode. The top geometry (a) is for the ideal case in which the electron beam size is much smaller than the mode wavelength. The bottom geometry (b) shows a real electron beam with non-negligible diameter; the detail to the right shows the relative coupling different portions of the electron beam to different phases of the driven wave.

the electron beam couples energy into the waveguide mode over a range of phase angles [Fig. 3(b)]. The phase angle ϕ varies by $\pm\omega z_b/c$ over the longitudinal electron beamwidth z_b. Rewriting this phase angle in terms of an effective phase delay time $\tau_p = z_b/c$ yields $\phi = \omega\tau_p$. Averaging over this range of phase angles is now equivalent to averaging (1) over an effective phase delay time τ_p,

$$\frac{1}{\tau_p}\int_{-\tau_p/2}^{\tau_p/2}\frac{\sin(\omega\tau_t/2)\cos(\omega t)}{\omega\tau_t/2}dt = \frac{\sin(\omega\tau_t/2)}{\omega\tau_t/2}\frac{\sin(\omega\tau_p/2)}{\omega\tau_p/2} . \quad (2)$$

Figure 4 displays the power spectrum for a 1-mm and a 2-mm electron beam diameter crossing a guide with a 6-ps transit time (waveguide cutoff is ignored for this example). Note that the effect of the electron beamwidth becomes important when the transit time and the electron phase time are of the same order.

C. Higher-order mode-coupling effects

Limiting waveguide coupling analysis to only uniform field E_y across the center of the waveguide (TE_{10} coupling) is not valid because of the broadband nature of the electron signal. From waveguide theory, the TE_{mn} electric field across a waveguide (parallel to the electron velocity) is proportional to [19]

$$E_y \propto \sin(m\pi x/a)\cos(n\pi y/b) . \quad (3)$$

Adding a higher-order mode term to (1) yields the coupling equation for any TE_{1n} mode (at $x = a/2$, the waveguide center),

$$\frac{1}{\tau_t}\int_{-\tau_t/2}^{\tau_t/2}\cos\left[\frac{n\pi y}{b}\right]\cos(\omega t+\phi)dt = \left\{\frac{\sin[(n\pi/2)+\omega\tau_t/2]}{n\pi+\omega\tau_t} + \frac{\sin[(n\pi/2)-\omega\tau_t/2]}{n\pi-\omega\tau_t}\right\}\cos(\phi) , \quad (4)$$

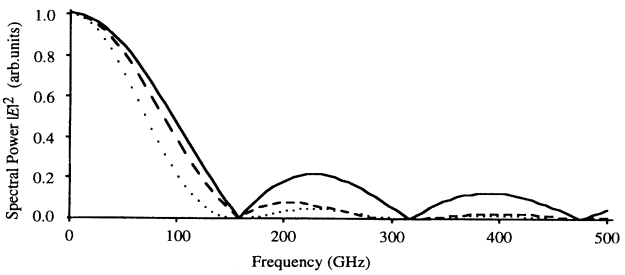

FIG. 4. Frequency response for wide electron beams crossing a waveguide. All plots are for an electron beam with 6-ps transit time. Solid curve, ideal beam, $\tau_p = 0$; dashed curve, 1 mm beam diameter, $\tau_p = 3.3$ ps; dotted curve, 2 mm beam, $\tau_p = 6.6$ ps.

where $y = tb/\tau_t$ and b is the waveguide height. Figure 5(a) shows the magnitude of the coupling for TE_{10}, TE_{11}, and TE_{12} modes. Correcting (4) for a non-negligible beamwidth as in (2) yields

$$\left\{\frac{\sin[(n\pi/2)+\omega\tau_t/2]}{n\pi+\omega\tau_t} + \frac{\sin[(n\pi/2)-\omega\tau_t/2]}{n\pi-\omega\tau_t}\right\}\frac{\sin(\omega\tau_p/2)}{\omega\tau_p/2} . \quad (5)$$

Figure 5(b) shows the power spectrum due to the sum of the three fields, corrected for mode cutoff, for both a negligible beamwidth and a 1-mm beam diameter. Higher-order wavelength modes and the non-negligible electron beam diameter have a considerable effect on the spectrum produced in the waveguide. The waveguide geometry of Fig. 2 will yield a response spectrum similar to the one shown in Fig. 5(b).

D. Field sampling: Transverse waveguide pickup

For the case in which the electron bunches travel coaxially in a beam pipe, the fields at the beam pipe wall at $z = 0$ are related to the electron bunch distribution $\Lambda(t)$ by

$$\vec{H}(r,t) = \frac{q\Lambda(t)}{2\pi r\sqrt{\varepsilon_0\mu_0}}\hat{\varphi}, \quad \vec{E}(r,t) = \frac{q\Lambda(t)}{2\pi\varepsilon_0 r}\hat{r} , \quad (6)$$

where r is the radial position, q is the electron charge,

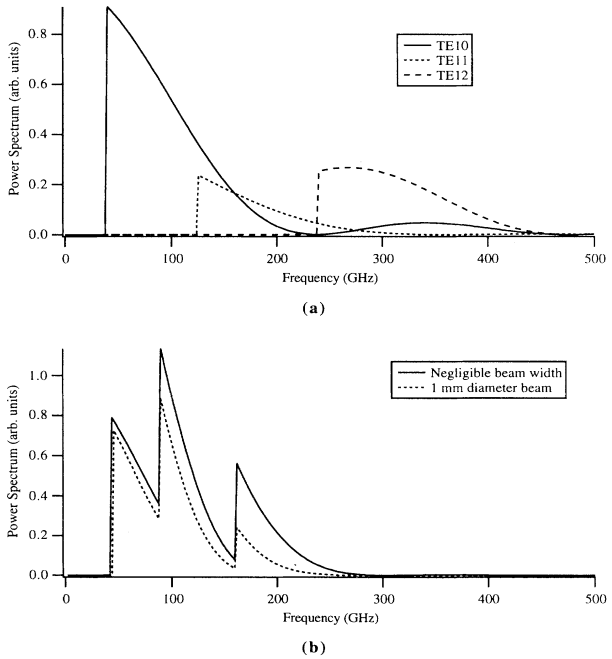

FIG. 5. Waveguide coupling of TE_{1n} modes. (a) Field coupling for TE_{10}, TE_{11}, and TE_{12} modes. (b) Power spectrum of the sum of the three modes for a beam of negligible beamwidth and 1 mm beam diameter. Breaks in both curves indicate the mode cutoff frequency. (Model waveguide dimensions 2×4 mm^2.)

and ε_0 and μ_0 are permittivity and permeability. Fourier transforming (6) yields the rf spectrum produced by the bunch passing $z=0$,

$$\tilde{H}(r,\omega)=\int_{t=-\infty}^{\infty}\vec{H}(r,t)\exp(-j\omega t)dt$$
$$=\frac{q}{2\pi r\sqrt{\mu_0\varepsilon_0}}\tilde{\Lambda}(\omega)\hat{\varphi}\ , \tag{7}$$

where $\tilde{\Lambda}(\omega)$ is the Fourier transform of $\Lambda(t)$.

The frequency response of the rectangular waveguide pickup, shown in Fig. 1, is found using a theory of field equivalence at an aperture [12,20]; the waveguide field must satisfy

$$\hat{n}\times\vec{H}_{\rm WG}=\vec{J}_c=\hat{n}\times\vec{H}_{\text{electron beam}} \tag{8}$$

across the aperture formed by the waveguide entrance at the beam pipe radius. From (8) the field initially launched into the pickup waveguide has a temporal evolution directly related to the relativistic electron bunch duration. Using Faraday's law, the electric field launched into the pickup and subsequently characterized is

$$\vec{\nabla}\times\vec{E}_{\rm WG}=-\mu_0\frac{\partial}{\partial t}\vec{H}_{\rm WG}\ , \tag{9}$$

which, combined with (8) and (6), yields

$$\vec{E}_{\rm WG}\propto-\mu_0\frac{\partial}{\partial t}\vec{J}_c\propto\frac{\partial}{\partial t}\Lambda(t)\hat{z}\ . \tag{10}$$

The electron bunches that travel along the beam pipe will have a nonzero transverse dimension. Hence, when a bunch passes the waveguide pickup, the field produced by electrons in the transverse plane further from the pickup will produce a field retarded in time. As a result, the rf signal at the pickup will be the convolution of the axial electron density and the transverse density function.

E. Electron bunch timing

Equations (7) and (10) predict that the frequency spectrum of the fields generated by the electron bunch observed in the laboratory frame is directly related to the laboratory frame spatial charge distribution. Shortening the bunch duration will broaden the observed spectrum. As an example, rectangular bunches with 2 ps duration will have spectral extent greater than 250 GHz.

In our experiments, instead of a single bunch, many bunches are periodically launched through the beam pipe. For analytic simplicity, the individual bunch shapes and the period between bunches are assumed to be constant. This assumption is valid because the response time of the detection system is long compared to the bunch period; hence the measured bunch shape is the average over many bunches. Mathematically, the field in the beam pipe (at $z=0$) is the convolution of (6) with an impulse train of period τ,

$$\vec{H}_m(r,t)=\mathcal{R}_\tau(\vec{H}(r,t))=\frac{q}{2\pi r\sqrt{\varepsilon_0\mu_0}}\hat{\varphi}\sum_{n=-\infty}^{\infty}\Lambda(t-n\tau)\ , \tag{11}$$

where $\vec{H}(r,t)$ is the single bunch field given by (6) (the subscript m indicates that the field is due to a train of single bunches or "micropulses" represented by function R). The Fourier transform of this periodic field is no longer continuous, as in the single pulse case, but is instead made up of discrete impulses, spaced by $1/\tau$. Mathematically, the spectrum is written as

$$\tilde{H}_m(\omega)=\frac{1}{\tau}\mathcal{C}_{1/\tau}(\tilde{H}(\omega))$$
$$=\frac{1}{\tau}\frac{q}{2\pi r\sqrt{\varepsilon_0\mu_0}}\hat{\varphi}\tilde{\Lambda}(\omega)\sum_{n=-\infty}^{\infty}\delta\left[\omega-\frac{2\pi n}{\tau}\right]\ , \tag{12}$$

where C is a comb of equally spaced frequencies. This is the discrete spectrum that is delivered to and measured by the spectrometer system.

The actual beam of electron bunches measured in this work is modulated (Fig. 6) by a periodic rectangular pulse. The modulation produces trains of electron bunches ("macropulses"); the bunch train is of 1–4 μs duration. To measure the field produced, the detector signal is sampled only during the macropulse period. This sampling improves the autocorrelation (rms) signal-to-noise ratio by the ratio of the chopping period T_M to the pulse sample width T_D [21],

$$\frac{(S/N)_{\rm sampled}}{(S/N)_{\rm averaged}}\approx\left[\frac{T_M}{T_D}\right]^{1/2}\ . \tag{13}$$

For this research, $T_M\approx0.1$ s and $T_D\approx1$ μs, giving a (rms) signal-to-noise ratio improvement of $\sim10^2$–10^3 when sampling.

F. Waveguide coupling and signal transmission theory

Although (10) describes the field launched into the waveguide pickup, the waveguide restricts the spectrum of the field that propagates. The low-frequency cutoff f_c of the sampling waveguide is determined by

$$f_c=\sqrt{(m/w)^2+(n/h)^2}/2\sqrt{\mu\varepsilon}\ , \tag{14}$$

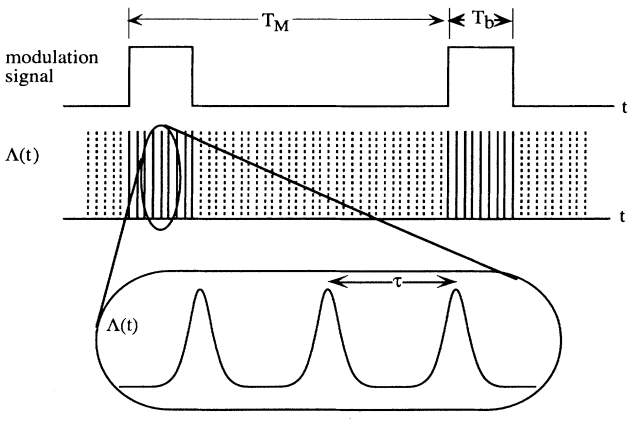

FIG. 6. Electron beam bunch timing showing the modulation of the periodic electron bunches.

where m and n are the mode indices for the TE_{mn} and TM_{mn} modes. Applying (14) to the dimensions of the pickup waveguide used in this work ($w=3.81$ mm and $h=1.27$ mm), the lowest-order mode (TE_{10}) has a cutoff of 39.4 GHz and the next lowest cutoff (TE_{20}) is at 78.7 GHz.

G. Waveguide attenuation and dispersion characteristics

In the experiments described here, the e.m. pulse produced by the electron bunch is transmitted from the pickup to the measurement equipment through overmoded waveguide. This transmission waveguide produces little attenuation but the dispersion is quite large [22]; fortunately, the measurement techniques used in these experiments are insensitive to phase and have a frequency resolution too low to observe dispersion. We treat the measured pulse as a bandwidth limited pulse.

H. Fourier transform spectroscopy theory

A Fourier transform spectrometer (FTS) [23–27] was used for all electron beam signal measurements. Because the functions of autocorrelation and power spectra are Fourier transform pairs

$$f(t)\oplus f(t)\Longleftrightarrow |F(\omega)|^2 , \tag{15}$$

we can view this spectrometer as producing frequency domain power spectra or as producing time domain, autocorrelation measurements. Depending on the information required, one domain will often give more insight into the nature of the signal. Both time and frequency domain characteristics are used in this project.

The signal produced by the interferometer is [22]

$$D(t,\delta)-\tfrac{1}{2}D(t,0) = 2\,\mathrm{Re}\left\{\int_{\tau=-\infty}^{\infty} h(t-\tau)E^*(\tau)E(\tau-2\delta/c)d\tau\right\} , \tag{16}$$

where $D(t,\delta)$ is the FTS detector output as a function of time and mirror displacement δ (Fig. 7), $E(t)$ is the transient signal from the electron bunch, and $h(t)$ is the detector temporal impulse response. By varying δ and sampling at the same time in the pulse train, (16) can be used to compute the electron bunch autocorrelation. In addition, by keeping δ fixed, the time evolution of (16) will be proportional to the pulse autocorrelation width variation during the pulse train. Both techniques are valuable diagnostics.

Taking the Fourier transform $\mathcal{F}$ of (16) yields the classical cw FTS relationship

$$|\tilde{E}(c\sigma)|^2 \propto \mathcal{F}\{\langle D(t,\delta)\rangle-\tfrac{1}{2}\langle D(t,0)\rangle\} . \tag{17}$$

The left-hand side of (17) is the power spectra of the incident signal as a function wave number σ. The argument of the Fourier transform on the right-hand side of (17) is the detector signal as a function of mirror displacement. It is important to note that the integrand in (17) is independent of any frequency-dependent phase variation in $\tilde{E}$. Hence a FTS is insensitive to any dispersion present in the source signal. Although methods exist for calculating the phase [28,29] information, they were not used in these experiments.

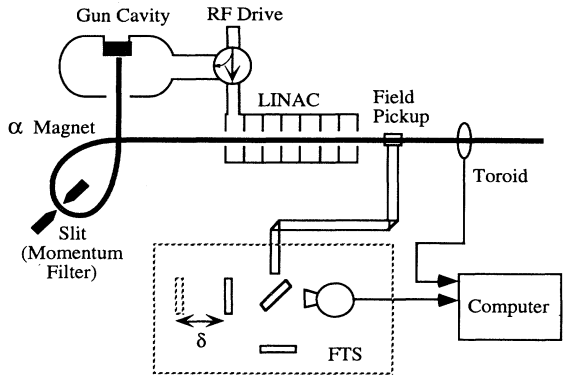

FIG. 7. Schematic of the Mark III electron beam system and the FTS measurement system; δ is the FTS mirror displacement and LINAC denotes the linear accelerator.

III. EXPERIMENTAL DESIGN

Two electron beam systems were evaluated in this study. The first device is the Duke University Mark III FEL [30], which generates a 40-MeV beam of picosecond duration electron bunches. The second electron beam source used in this work is a 1-MeV picosecond electron bunch source (PEBS) [31]. In both systems, bunches arrive every 350 ps. The periodic train of picosecond electron bunches is not continuous; rather it is modulated to produce trains of electron bunches of 1–4 μs in duration at a rate of 10 Hz (Fig. 6). Figure 7 is a schematic of the Mark III electron beam system and the FTS sampling and analysis hardware. The experimental setup for the 1-MeV system was similar, lacking only the linear accelerator section.

The sampling pickup in the Mark III was a simple rectangular waveguide stub, finished flush with the wall of the electron beam pipe (Fig. 1). This waveguide had a 39.4-GHz cutoff and 4-ps transit time. In the PEBS study, the electron beam crossed the center of a rectangular waveguide with a 40-GHz cutoff and 6-ps transit time. In both studies, an overmoded waveguide brought the microwave beam into the spectrometer. In the FEL experiments the overmoded transport waveguide was 20 m long and in the PEBS experiments the transport system was 1 m long. Because the transport waveguide in both systems produced low, uniform loss across the spectrum of interest, the overall transport waveguide length did not affect the measurements.

The FTS was of conventional design [23] and used a commercial translation stage, a stepper motor, and front surface aluminized mirrors. Mylar beam splitters of 50 and 250 μm thicknesses were used depending on signal bandwidth and power. The detector was a helium-cooled InSb hot-electron bolometer with a video impulse response greater than 2 MHz. The spectral response, shown in Fig. 8, of the FTS was calibrated with a black-

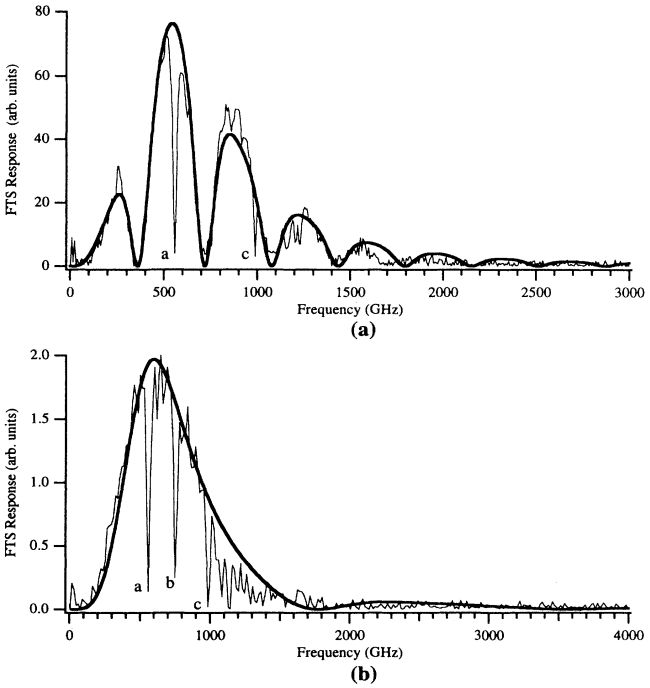

FIG. 8. Blackbody spectral response of the FTS and the fit to the theoretically system model for (a) 250-μm and (b) 55-μm beam splitters. The bold curve is the model, the single width curve is the experimental data. Letters at absorption peaks indicate water absorption lines (see the text).

body source. The blackbody calibration data allow us to compensate the measured data for the FTS system response. Also, the strong water vapor absorption lines (at 557, 752, and 988 GHz, labeled *a*, *b*, and *c* in Fig. 8) verify the frequency accuracy of the FTS system.

IV. RESULTS AND DISCUSSION

Figure 9 shows a typical autocorrelation of the rf pulse generated by the 40-MeV electron bunch. The solid curve is a theoretically predicted response for a Gaussian pulse with 2.1-ps full width at half maximum (FWHM). The figure clearly shows an excellent fit to the central interferogram peak. Figure 10 shows the estimated

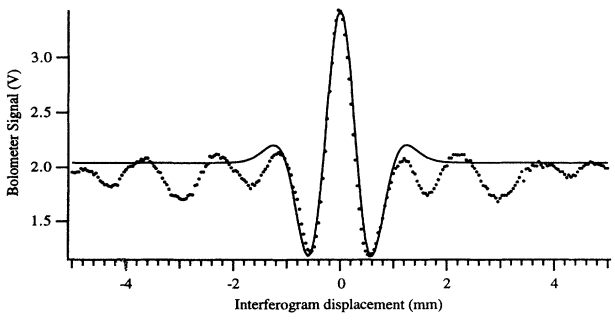

FIG. 9. Measured (dots) and predicted (solid) interferogram data from the Duke University Mark III FEL. The predicted fit is for a 2.1-ps FWHM Gaussian pulse.

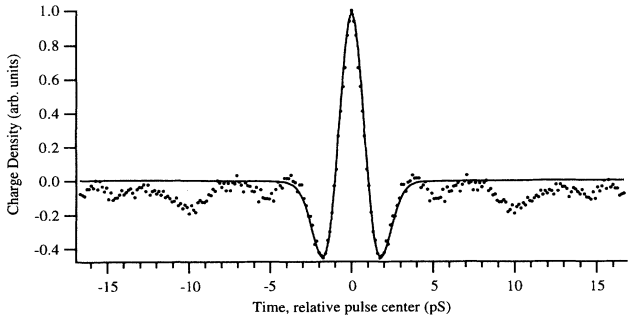

FIG. 10. Calculated decorrelation of data in Fig. 9. Experimental data (squares) and predicted (solid) data for a 2.1-ps FWHM Gaussian pulse.

"decorrelated" electron bunch density and the theoretical response for the Gaussian distribution. The negative going sidelobes are due to the high-pass response of the FTS. The variations in measured bunch density away from the pulse center are thought to be due to stray electrons that lead or lag the main pulse.

Figure 11 shows the rf spectrum produced by the electron bunch transient, in addition to the FTS response and the spectrum predicted by the higher-order mode model for TE_{10}, TE_{11}, TE_{12}, and TE_{13} modes. The computation of the spectrum used a simple Hanning window to reduce spectral leakage and averaged three interferograms to improve the signal-to-noise ratio. Although the FTS response at low frequencies complicates the comparison of the measured data and predicted data, the measured data show peaks near those predicted by the higher-order mode analysis (e.g., the periodic structure in the wings of the time domain autocorrelation spaced at 1.2 mm correspond to the spectral peak near 250 GHz). The sample-to-sample noise in the interferogram is thought to be due to position or energy changes in the electron beam during measurement. Monitoring the toroid current during macropulses indicates a correlation between the interferogram sample-to-sample noise and beam fluctuations. The current sampling hardware limits the FTS data rate to about one sample a second; a 1024 sample interferogram

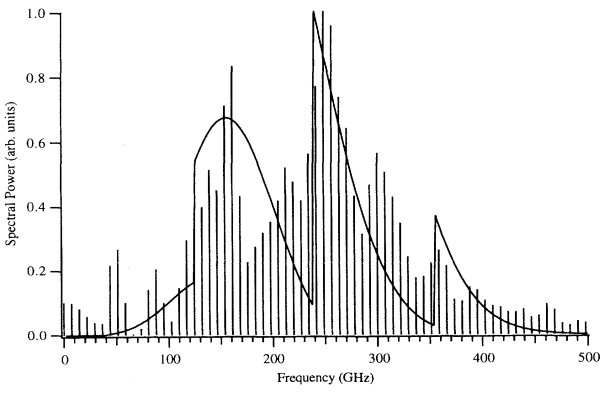

FIG. 11. Power spectrum of the measured pulse (histogram) and the predicted spectrum (solid curve) based on the higher-order mode coupling model.

requires over 17 min to collect, a time scale over which significant electron beam system drifts occur. Averaging multiple interferograms improves the signal-to-noise ratio at the expense of longer measurement times.

Because the detector used in this project has sufficient speed to track the macropulse evolution, we are able to measure the micropulse interferogram at the beginning and end of a macropulse. To minimize effects of electron beam drifts, short scans (64 samples) centered on the interferogram peak were taken. Figure 12 compares the micropulse interferograms at the beginning and end of the macropulse at different linear accelerator rf drive levels. Figure 12 shows that the micropulse changes over the duration of the macropulse and the variation is sensitive to small changes in liner accelerator rf drive level. When these scans were acquired, the FEL would lase only in the +0.2-dBm rf drive setting, and then over only a portion of the macropulse. This indicates that the electron bunch evolution during the macropulse is significant to laser operation.

The Mark III electron beam was monitored over several months, including before and after major electron gun modifications. Figure 13 shows the measured pulse before (4.3-ps FWHM) and after (2.1-ps FWHM) the modifications. The FTS measurements immediately show that the rebuilt electron gun produced shorter bunches than the previous design. It is important to note the differences in interferogram structure between the two pulses is due entirely to the electron bunch and not the FTS impulse response. Comparing Fig. 9 to Fig. 13 shows that the overall structure of the interferogram is not due to the FTS, but is instead a function of the electron bunch shape and duration. These results show that the FTS is useful as a long term monitor of electron bunch performance.

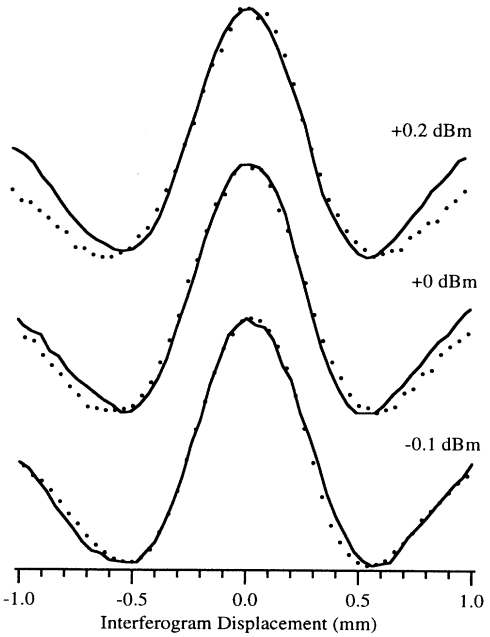

FIG. 12. Interferogram of bunches at macropulse times of 1.0 μs (dots) and 3.2 μs (solid line) at three different linear accelerator rf drive settings (-0.1, 0, and +0.2 dBm).

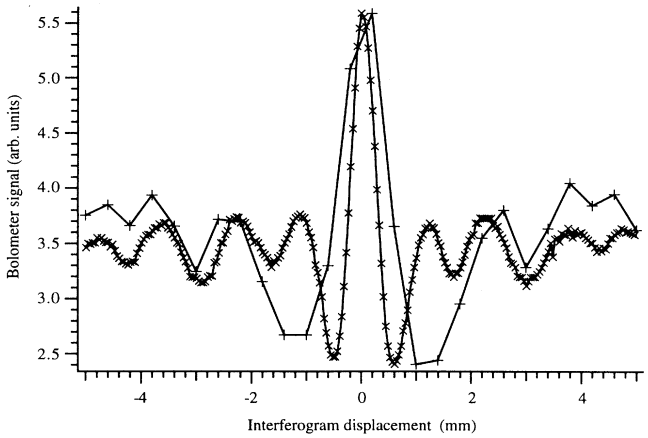

FIG. 13. Measurement of the electron bunch length before (+++) and after (×××) the Mark III electron gun modifications.

In another set of measurements, conducted on the PEBS, the alpha magnet momentum filter (MF) was adjusted between FTS scans. The momentum filter selects the energy spread of the electron beam. Increasing the energy spread will increase the electron bunch length. The FTS scans shown in Fig. 14 measure a clear increase in electron bunch length as the MF setting increases. These measurements again validate the use of FTS as real-time beam diagnostic.

Finally, the PEBS system was used to check the waveguide coupling model, which includes higher-order mode coupling and a non-negligible electron beam diameter. Figure 15 shows the measured spectrum along with the predicted spectrum. Adjusting only the predicted amplitude yields a very good fit to the measured data. The slight shift in cutoff frequencies is assumed to be due to minor inaccuracies in the waveguide machining.

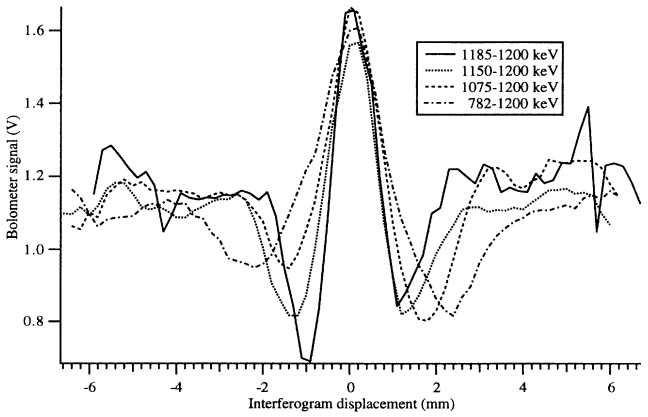

FIG. 14. Pulse width change due to the increase of electron bunch energy spread. Momentum filter settings (MF) are 1185–1200 keV (solid line), 1150–1200 KeV (dotted line), 1075–1200 KeV (dashed line), and 782–1200 KeV (dot-dashed line).

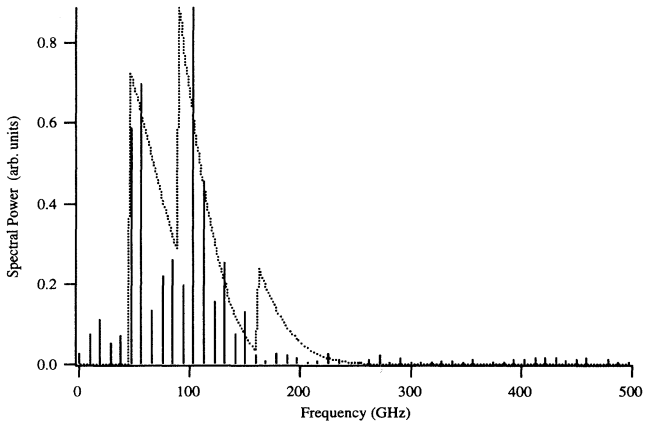

FIG. 15. Measured spectrum (histogram) of the rf produced by an electron beam passing a rectangular waveguide. The dotted curve is the spectrum predicted by the waveguide coupling model incorporating higher-order modes and 1 mm diameter beam.

Overall these measurements validate the higher-order mode coupling model.

V. CONCLUSIONS

This research has shown that a broadband rf pickup and FTS based measurement system forms a simple, noninvasive technique for pulsed electron beam diagnostics. This technique has picosecond temporal resolution [measuring 2.1-ps (FWHM) electron bunches], provides both long-term and real-time characterizations, and allows the study of electron bunch evolution over microsecond periods. Although the measurement approach has been verified on linear electron beam systems, the noninvasive techniques will find great utility in electron bunch storage rings, where destructive diagnostics would require refilling the ring.

Currently the temporal resolution is limited by the frequency-dependent response of the FTS and the pickup. Replacing the dielectric beam splitter in the FTS with wire mesh beam splitters will flatten the FTS response and extend the submillimeter wavelength range. This modification will allow the measurement of subpicosecond transients.

The complicated response of the pickup geometry also limits the temporal resolution. Simply using smaller pickup waveguide will reduce higher-order mode coupling effects at the cost, however, of signal power. Another alternative would be to use a pickup waveguide that suppresses higher-order mode coupling. These alternatives are currently under investigation.

From an operational standpoint, the sampling hardware and FTS scanning system were too slow to optimally measure the 10-Hz-modulated FEL electron beam. An improved FTS system would incorporate sampling hardware with sufficient speed and memory to sample and store a complete autocorrelation scan. In addition, the FTS mirror scanning system would be synchronized to the electron beam modulator timing so that the scanning mirror would be automatically translated between each sample. These modifications will allow faster scans and will reduce the impact of electron beam system drift on the FTS measurements.

The InSb bolometer used for this paper was overly sensitive for the signals generated by the electron beams. Although care was taken to stay in the linear regime of detector operation, the InSb bolometer used in these experiments operated near saturation. In addition, the InSb bolometer response time was only sufficient to resolve changes in the beginning and end of the 4-μs macropulse. To overcome these limitations, we are characterizing submillimeter detectors that have faster response times and lower sensitivity. The ideal detector for this work would have a nanosecond response time and a responsivity of a few volts per watt at 30 cm^{-1}.

Although this research has monitored the electron bunch characteristics at a single point in the electron beam line, noninvasive FTS-based measurements allow the analysis of the electron beam at several points along the beam line. Such a study would provide information about the electron bunch evolution as it travels through a FEL or storage ring. As a diagnostic, this approach would give electron beam system operators a tool for monitoring and characterizing system performance without deleterious system perturbation.

ACKNOWLEDGMENTS

This work was supported by the U.S. Army Research Office, Grants Nos. DAAL03-89-D-0002-0001 and DAAH 04-93-G-0230, and by the Air Force Office of Scientific Research, Grant No. F49620-89-C-0062. The authors would like to thank John Madey, Dave Straub, and Eric Szarmes for their insightful discussions and access to the Duke University Mark III FEL.

[1] M. G. Billing, Nucl. Instrum. Methods Phys. Res. Sect. A **266**, 144 (1988).
[2] R. Bergere, A. Veyssiere, and P. Daujat, Rev. Sci. Instrum. **33**, 1441 (1962).
[3] R. W. Coombes and D. Neet, IEEE Trans. Nucl. Sci. **14**, 1111 (1967).
[4] J.-C. Denard, G. Oxoby, J.-L. Pellagrin, and S. Williams, IEEE Trans. Nucl. Sci. **NS-30**, 2364 (1983).
[5] E. V. Farinholt, Z. D. Farkas, and H. A. Hogg, IEEE Trans. Nucl. Sci. **14**, 1127 (1967).
[6] S. P. Jachim, R. C. Webber, and R. E. Shafer, IEEE Trans. Nucl. Sci. **NS-28**, 2323 (1981).
[7] B. Kulke, H. Shay, F. Coffield, R. Frye, and R. Holmes, Nucl. Instrum. Methods Phys. Res. Sect. A **272**, 241 (1988).
[8] R. B. Neal, *The Stanford Two Mile Accelerator* (Benjamin, New York, 1968).
[9] R. E. Shafer, IEEE Trans. Nucl. Sci. **NS-32**, 1933 (1985).
[10] H. Motz, W. Thon, and R. N. Whitehurst, J. Appl. Phys. **24**, 826 (1953).

[11] H. Motz, J. Appl. Phys. **22**, 527 (1951).
[12] J. D. Jackson, *Classical Electrodynamics* (Wiley, New York, 1975).
[13] K. J. Kleman, Nucl. Instrum. Methods Phys. Res. Sect. A **266**, 172 (1988).
[14] E. L. Brodsky, K. J. Klemen, G. Rogers, D. Rioux, R. Patel, and H. Hochst, Rev. Sci. Instrum. **63**, 519 (1992).
[15] Y. Shibata, T. Takahashi, T. Kanai, M. Ishi, M. Ikezawa, J. Ohkuma, S. Okuda, and T. Okada, Phys. Rev. E **50**, 1479 (1994).
[16] T. Takahashi, Y. Shibata, F. Arai, K. Ishi, T. Ohsaka, M. Ikezawa, Y. Kondo, T. Nakazato, S. Urasawa, R. Kato, S. Niwano, and M. Oyamada, Phys. Rev. E **48**, 4674 (1993).
[17] P. Kung, H.-C. Lihn, H. Wiedemann, and D. Bodek, Phys. Rev. Lett. **73**, 967 (1994).
[18] J. C. Sheppard, J. E. Clendenin, M. B. James, R. H. Miller, and M. C. Ross, IEEE Trans. Nucl. Sci. **NS-32**, 2006 (1985).
[19] S. Ramo, J. R. Whinnery, and T. Van Duzer, *Fields and Waves in Communications Electronics* (Wiley, New York, 1984).
[20] R. E. Collin, *Field Theory of Guided Waves* (McGraw-Hill, New York, 1960).
[21] F. G. Stremler, *Introduction to Communication Systems* (Addison-Wesley, Reading, MA, 1982).
[22] J. C. Swartz, Ph.D. thesis, Duke University, 1994 (unpublished).
[23] R. J. Bell, *Introductory Fourier Transform Spectroscopy* (Academic, New York, 1972).
[24] R. D. Guenther, *Modern Optics* (Wiley, New York, 1990).
[25] J. Connes, Rev. Opt. Théor. Instrum. **40**, 45 (1961); **40**, 116 (1961); **40**, 171 (1961); **40**, 231 (1961).
[26] J. Connes and P. Connes, J. Opt. Soc. Am. **56**, 896 (1966).
[27] D. H. Martin, in *Infrared and Millimeter Waves,* edited by K. Button (Academic, New York, 1982).
[28] R. Lai, U. Happek, and A. J. Sievers, Phys. Rev. E **50**, R4294 (1994).
[29] R. Lai and A. J. Sievers, Phys. Rev. E **50**, R3342 (1994).
[30] S. V. Benson, J. Schultz, B. A. Hooper, R. Crane, and J. M. J. Madey, Nucl. Instrum. Methods Phys. Res. Sect. A **272**, 22 (1988).
[31] C. R. Jones, M. J. Peters, and J. M. Dutta, in *The International Society for Optical Engineering, Conference Digest: 17th International Conference on Infrared and Millimeter Waves,* edited by Richard J. Temkin, SPIE Proc. Vol. 1929 (SPIE, Bellingham, WA, 1992), pp. 138–139.

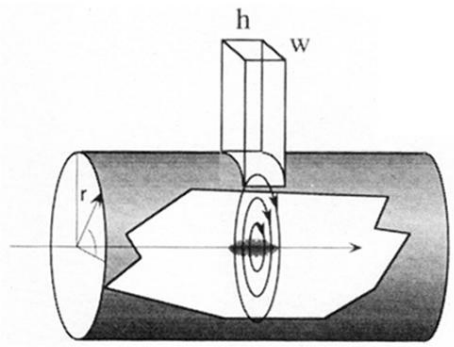

FIG. 1. Waveguide geometry for the coupling rf from a cylindrical electron beam pipe into a rectangular pickup with height h and width w.

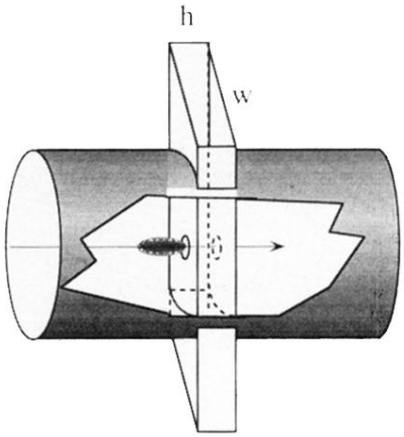

FIG. 2. Waveguide geometry for the coupling rf from an electron bunch traversing a rectangular waveguide with height h and width w.